PPPL-2310

ANOMALOUS THERMAL CONFINEMENT IN OHMICALLY HEATED TOKAMAKS

By

F. Romanelli, W.M. Tang, and R.B. White

FEBRUARY 1986

PLASMA
PHYSICS
LABORATORY

PRINCETON UNIVERSITY
PRINCETON, NEW JERSEY

PREPARED FOR THE U.S. DEPARTMENT OF ENERGY,
UNDER CONTRACT DE-AC02-76-CHO-3073.

EXTERNAL DISTRIBUTION IN ADDITION TO UC-20

Plasma Res Lab, Austra Nat'l Univ, AUSTRALIA
Dr. Frank J. Paoloni, Univ of Wollongong, AUSTRALIA
Prof. I.R. Jones, Flinders Univ., AUSTRALIA
Prof. M.H. Brennan, Univ Sydney, AUSTRALIA
Prof. F. Cap, Inst Theo Phys, AUSTRIA
Prof. Frank Verheest, Inst theoretische, BELGIUM
Dr. D. Palumbo, Dg XII Fusion Prog, BELGIUM
Ecole Royale Militaire, Lab de Phys Plasmas, BELGIUM
Dr. P.H. Sakanaka, Univ Estadual, BRAZIL
Dr. C.R. James, Univ of Alberta, CANADA
Prof. J. Teichmann, Univ of Montreal, CANADA
Dr. H.M. Skarsgard, Univ of Saskatchewan, CANADA
Prof. S.R. Sreenivasan, University of Calgary, CANADA
Prof. Tudor W. Johnston, INRS-Energie, CANADA
Dr. Hannes Barnard, Univ British Columbia, CANADA
Dr. M.P. Bachynski, MPB Technologies, Inc., CANADA
Chalk River, Nucl Lab, CANADA
Zhengwu Li, SW Inst Physics, CHINA
Library, Tsing Hua University, CHINA
Librarian, Institute of Physics, CHINA
Inst Plasma Phys, Academia Sinica, CHINA
Dr. Peter Lukac, Komenskeho Univ, CZECHOSLOVAKIA
The Librarian, Culham Laboratory, ENGLAND
Prof. Schatzman, Observatoire de Nice, FRANCE
J. Radet, CEN-BP6, FRANCE
AM Dupas Library, AM Dupas Library, FRANCE
Dr. Tom Mual, Academy Bibliographic, HONG KONG
Preprint Library, Cent Res Inst Phys, HUNGARY
Dr. R.K. Chhajlani, Vikram Univ. INDIA
Dr. B. Dasgupta, Saha Inst, INDIA
Dr. P. Kaw, Physical Research Lab, INDIA
Dr. Phillip Rosenau, Israel Inst Tech, ISRAEL
Prof. S. Cuperman, Tel Aviv University, ISRAEL
Prof. G. Rostagni, Univ Di Padova, ITALY
Librarian, Int'l Ctr Theo Phys, ITALY
Miss Clelia De Palo, Assoc EURATOM-ENEA, ITALY
Biblioteca, del CNR EURATOM, ITALY
Dr. H. Yamato, Toshiba Res & Dev, JAPAN
Direc. Dept. Lg. Tokamak Dev. JAERI, JAPAN
Prof. Nobuyuki Inoue, University of Tokyo, JAPAN
Research Info Center, Nagoya University, JAPAN
Prof. Kyoji Nishikawa, Univ of Hiroshima, JAPAN
Prof. Sigeru Mori, JAERI, JAPAN
Prof. S. Tanaka, Kyoto University, JAPAN
Library, Kyoto University, JAPAN
Prof. Ichiro Kawakami, Nihon Univ, JAPAN
Prof. Satoshi Itoh, Kyushu University, JAPAN
Dr. D.I. Choi, Adv. Inst Sci & Tech, KOREA
Tech Info Division, KAERI, KOREA
Bibliotheek, Fom-Inst Voor Plasma, NETHERLANDS
Prof. B.S. Liley, University of Waikato, NEW ZEALAND
Prof. J.A.C. Cabral, Inst Superior Tecn, PORTUGAL
Dr. Octavian Petrus, ALI CUZA University, ROMANIA
Prof. M.A. Hellberg, University of Natal, SO AFRICA
Dr. Johan de Villiers, Plasma Physics, Nucor, SO AFRICA
Fusion Div. Library, JEN, SPAIN
Prof. Hans Wilhelmson, Chalmers Univ Tech, SWEDEN
Dr. Lennart Stenflo, University of UMEA, SWEDEN
Library, Royal Inst Tech, SWEDEN
Centre de Recherchesen, Ecole Polytech Fed, SWITZERLAND
Dr. V.T. Tolok, Kharkov Phys Tech Ins, USSR
Dr. D.D. Ryutov, Siberian Acad Sci, USSR
Dr. G.A. Eliseev, Kurchatov Institute, USSR
Dr. V.A. Glukhikh, Inst Electro-Physical, USSR
Institute Gen. Physics, USSR
Prof. T.J.M. Boyd, Univ College N Wales, WALES
Dr. K. Schindler, Ruhr Universitat, W. GERMANY
Nuclear Res Estab, Julich Ltd, W. GERMANY
Librarian, Max-Planck Institut, W. GERMANY
Bibliothek, Inst Plasmaforschung, W. GERMANY
Prof. R.K. Janev, Inst Phys, YUGOSLAVIA

ANOMALOUS THERMAL CONFINEMENT IN OHMICALLY HEATED TOKAMAKS

F. Romanelli,‡ W. M. Tang, and R. B. White

Plasma Physics Laboratory, Princeton University

P.O. Box 451

Princeton, New Jersey 08544

PPPL--2310

DE86 007528

ABSTRACT

A model is proposed to explain the behavior of the gross energy confinement time in ohmically heated tokamak plasmas. The analysis takes into account the effect of the anomalous thermal conductivity due to small scale turbulence and of the macroscopic MHD behavior, which provides some constraints on the temperature profile. Results indicate that the thermal conductivity associated with the dissipative trapped-electron mode and with the ion temperature gradient (η_i) mode can account, respectively, for the Neo-Alcator scaling and the saturation of the energy confinement time with density. Comparisons with experimental results show reasonable agreement.

‡Permanent address: Associazione Euratom-Enea sulla Fusione, Centro Ricerche Energia, Frascati, Rome (Italy)

I. INTRODUCTION

To gain an understanding of the thermal confinement properties in tokamak plasmas has been the principal goal of many theoretical and experimental investigations. In particular, the experimental observation that the energy confinement time τ_E increases linearly with the average density [1] has stimulated attempts to explain this trend as well as further investigations of possible scalings of τ_E with other key plasma parameters and with the size of the device [2,3]. This has involved comparisons of results from different experiments and also confinement studies carried out on a single machine [4-9]. The data base from these studies, which have been recently summarized in Refs. 10 and 11 indicates that at low density in ohmic discharges, τ_E is rather well described by the so-called "Neo-Alcator" scaling, $\tau_E \propto \bar{n}\, a^{1.04} R^{2.04}$, where $\bar{n}$ is the line average density, a is the minor radius, and R is the major radius. However, at higher densities this improvement of τ_E with density tends to disappear. Specifically, on ISX-A [4] it was found that the saturation of τ_E with $\bar{n}$ was followed by some degradation with further increase in density. This behavior was explained by the onset of the neoclassical ion thermal losses. Although a similar trend was observed on Doublet III, the density at saturation was observed to be well below the density at which neoclassical theory [12,13] predicts the ion losses to be important. In higher field machines the change in the scaling of τ_E on density was found to be less dramatic. Nevertheless, while the results from Alcator A [14] and FT [9] were found to be in agreement with the prediction for saturation associated with ion neoclassical theory, the Alcator C [7] data showed an apparent disagreement.

Among the possible causes of the anomalous electron (and at times anomalous ion) thermal conductivity, attention has been focused on

electrostatic microinstabilities. A prominent class of such modes are the instabilities belonging to the drift branch driven by the presence of particles trapped in the local magnetic mirror of tokamak devices [15]. A large amount of work has been devoted to a proper description of these low frequency modes and has involved taking into account many physical effects (temperature gradients, finite ion Larmor radius, magnetic drift resonances, collisions, etc.) [16-19] as well as the effects of toroidal geometry on the structure of the eigenmodes. In particular, use of the ballooning representation [17] has led to considerable progress both analytically [18] and numerically [19]. At present the description of the linear properties of the instabilities in toroidal systems is quite comprehensive. However, the fundamental goal of understanding the anomalous thermal transport is still unresolved because a complete description of the nonlinear evolution of these modes has not yet been obtained.

In recent years a large amount of both theoretical and experimental work has been devoted to making progress in this area [20]. Because of the complexity of the problem, it is most realistic to turn to a "semi-empirical" approach. This basically involves empirically incorporating significant experimental trends into the theoretical model. The most relevant example of this kind of approach is the "principle of profile consistency" [21], which is based on the assumption that the experimentally measured thermal conductivities are those needed to reach a consistent set of temperature profiles. More recently, this prescription has been combined with the notion that the heat transport is mainly due to the dissipative trapped-electron modes in an important local region of the plasma [22, 23]. The local estimate for the electron thermal conductivity can be obtained from the familiar strong turbulence assumption, $\chi_e \sim \gamma/k_\perp^2$, with γ and $k_\perp$ being, respectively, the

linear growth rate and the perpendicular wave vector of the mode considered. At the simplest level for dissipative trapped-electron modes, $\gamma = \varepsilon^{3/2} \omega_n^* \omega_T^* / \nu_{ei}$ with $\varepsilon = r/R$, $\omega_n^* = (cT_e/eB)k_\perp |\nabla n/n|$, $\omega_T^* = \omega_n^* \, d \ln T / d \ln n$, and ν_{ei} is the electron-ion collision frequency. Hence

$$\chi_e = \frac{5}{2} \frac{\varepsilon^{3/2}}{k_\perp^2} \frac{\omega_n^* \omega_T^*}{\nu_{ei}} . \tag{1}$$

In previous work [23] it was shown that by assuming a Gaussian electron temperature profile, $T \propto \exp[-\alpha_T (r/a)^2]$ with α_T related to q_a by the Ohm's law, the electron energy balance equation can be solved to yield the following expression

$$\chi_e = \frac{58.6\times10^4}{n_o[10^{14}\,cm^{-3}]} \frac{a(cm)}{R^{1.9}(cm)} \frac{B^{1/3}(kG)}{q_a^{1.6}} \frac{\exp[2/3\alpha_q (r/a)^2] - \exp[-1/3\alpha_q (r/a)^2]}{(r/a)^2 [1-(r/a)^2]^{\alpha_n}} \tag{2}$$

with $\alpha_q \simeq q_a + 0.5$. To arrive at this result the entropy production (between the q = 1 and the q = 2 surface) calculated using Eqs. (1) and (2) are required to be the same. A particular appealing feature of this result for χ_e is that it basically leads to the Neo-Alcator scaling and is also in reasonable agreement with empirically determined forms of χ_e obtained from data analysis codes. Nevertheless, it is still necessary to demonstrate that the local expression for χ_e [given in Eq. (1)] together with appropriate conditions on χ_e outside of the region between q = 1 and q = 2 is, in fact, consistent with Eq. (2). In other words, within the framework of a global analysis, it is necessary to distinguish among different transport mechanisms which can be relevant in different regions of the plasma column. For example, the fact that in Eq. (1) χ_e vanishes both for $r \to 0$ and $r \to a$ indicates that

different models for the central region and for the edge are required.

The transport model presented in this paper incorporates three distinct processes which dominate, respectively, inside the q = 1 surface, between the q = 1 and the q = 2 surfaces, and beyond the q = 2 surface. In the first region a model for the m = 1 sawtooth is used in order to keep the temperature profile essentially flat in this region. The effect of the mode on the electric field is taken into account by defining an effective electric resistivity inside the q = 2 surface. In the second region the transport coefficient is given by $\chi = \chi^{ANOM} + \chi^{NC}$ with χ^{NC} being the neoclassical thermal conductivity (retained only for ions) and χ^{ANOM} associated with microinstabilities. For the electrons χ^{ANOM} is specified by Eq. (1), which, as already noted, leads to confinement time scaling in agreement with experimentally observed trends at low density. In order to study the problem of the saturation of the energy confinement time at high density, an anomalous conductivity due to the presence of the toroidal η_i mode (η_i = d ℓn T_i/d ℓn n) [24] is added to the neoclassical expression of the ion thermal conductivity. The notion that the η_i modes could play a role in the problem of the anomalous ion thermal conductivity is suggested by the observation that the experiments which indicate saturation in agreement with neoclassical theory are usually characterized by more peaked density profiles. This is the case, for example, in ISX-A [4], Alcator A [14], and FT [9]. Particularly interesting are the results of Alcator C. In the case where fairly broad density profiles are observed, i.e., $n = n_o(1-r^2/a^2)^{\alpha_n}$ with $0.5 < \alpha_n < 0.9$ [6,7], early saturation of τ_E with density is observed. However, considerably larger values of the energy confinement time have been obtained with pellet injection experiments which are characterized by more peaked density profiles [25]. The expression of the anomalous ion thermal conductivity is given by

$\chi_i^{ANOM} = (5/2)\gamma/k_\perp^2$ with γ estimated by the following expression

$$\gamma = \varepsilon_n^{1/2}\, \eta_i^{1/2}\, \omega_n^* \text{ with } \eta_i > \eta_{crit} \ ,$$

where $\varepsilon_n = L_n/R$, $L_n^{-1} = d\ell n\, n/dr$ and $\eta_{crit} \approx 1$ to 2.

At the edge of the plasma there are a number of mechanisms which could be responsible for the large value of the conductivity. For example, the influence of the m = 2 tearing mode, the presence of small-scale resistive instabilities, and radiation effects could all be relevant. Therefore, due to the complexity of the edge physics, the approach adopted here is to use the semi-empirical expression for the electron thermal conductivity given by Eq. (2) <u>for q > 2</u>. Although the transport mechanism invoked to derive Eq. (2) [i.e., the dissipative trapped electron mode] does not apply at the edge, it can nevertheless be justified by the following argument. The radial dependence of χ_e, as given by Eq. (2), is exactly the radial dependence which follows from the experimental observation of Gaussian temperature profiles and by the heat transport equation. Therefore, if the absolute magnitude of χ_e in any local region in the discharge is specified, then the global χ_e is determined. In Eq. (2) a local value of χ_e is determined by invoking the effect of the trapped-electron mode in the region between the q = 1 and q = 2 surfaces. Assuming that the profile consistency constraint is justified, the resultant global model can then be applied to the region outside of q = 2. The effect on the results of this choice for the edge model is discussed in Sec. IV.

For simplicity, the loss channels associated with radiation and charge exchange will be neglected. Moreover, the density profile is approximated by a generalized parabola, $n = n(0)\ (1-r^2/a^2)^{\alpha_n}$ with α_n ranging between 0.5 and

2. The remainder of this paper is organized as follows. In Sec. II the basic transport model is presented, and in Sec. III the MHD model is explained. The method of solution is examined in Sec. IV, and the results for low density and high density ohmic cases are also presented and discussed here. Concluding comments and a brief summary are given in Sec. V.

II. TWO FLUIDS TRANSPORT MODEL

The energy transport in a two-component plasma is described by the following differential equations

$$P_\Omega + P_{aux_e} - P_{ei} + \frac{1}{r}\frac{d}{dr} r n \chi_e \frac{dT_e}{dr} = 0$$

$$P_{ei} + P_{aux_i} + \frac{1}{r}\frac{d}{dr} r n \chi_i \frac{dT_i}{dr} = 0 \quad . \tag{3}$$

These represent a simplified pair of steady-state energy balance equations governing electrons and ions. Here T_e and T_i are the electron and ion temperatures, χ_e (χ_i) is the electron (ion) thermal conductivity, P_Ω is the ohmic power given by

$$P_\Omega = J_\parallel E_\parallel = \eta J_\parallel^2 \quad , \tag{4}$$

where η is the Spitzer resistivity with the neoclassical corrections

$$\eta = \frac{m_e}{ne^2\tau_e}\frac{\gamma(Z_{eff})}{f_{tr}} \quad , \tag{5}$$

$$f_{tr} = 1 - \frac{1.95\varepsilon^{1/2} - 0.95\varepsilon}{1+\nu_e^*} \quad ,$$

and

$$\gamma(Z_{eff}) = 0.29\ Z_{eff} + \frac{0.457\ Z_{eff}}{1.08+Z_{eff}} .$$

In Eq. (5) m_e is the electron mass, e is the electron charge, n is the density (assumed equal for electron and ions), and Z_{eff} is the effective ion charge. The factor f_{tr} is due to the presence of trapped particles, ε is the local inverse aspect ratio, $\varepsilon = r/R$, and $\nu_e^* \equiv \nu_{eff}/\omega_{be}$ with

$$\nu_e^* = \frac{R^{3/2}\ B_T\ Z_{eff}}{r^{1/2}\tau_e B_\theta (T_e/m_e)^{1/2}} \tag{6}$$

and

$$\tau_e = \frac{3\ m_e^{1/2}\ T_e^{3/2}}{4(2\pi)^{1/2}\ ne^4 \ell n\ \Lambda} ,$$

where $B_\theta (B_T)$ is the poloidal (toroidal) magnetic field and $\ell n\ \Lambda$ is the Coulomb logarithm. In the sawtooth region Eq. (5) cannot be applied without taking into account the effect of the mode on the electric field, which on average keeps the value of q at the center close to one. This effect is retained in our model by defining an effective resistivity given by

$$\eta_{eff}^{-1} = \sigma_{eff} = \sigma(r_1)\ g\left(\frac{r}{r_1}\right) + \left[1 - g\left(\frac{r}{r_1}\right)\right]\sigma(r) ,$$

where $\sigma = 1/\eta$ with η given by Eq. (5), r_1 is the radius of the q = 1 surface, and $g(x) = 1$ for $x < 1$ and $g(x) = 0$ for $x > 1$ (in order to avoid discontinuities in the numerical analysis a smooth function is chosen to approximate g; e.g., $g = \exp(-x^4)$. P_{ei} is the electron-ion collisional power transfer given by

$$P_{ei} = 3 \frac{m_e}{m_i} \frac{n}{\tau_e} (T_e - T_i) \tag{7}$$

and P_{aux_e} (P_{aux_i}) is the auxiliary power coupled to electrons (ions). Equations (5)-(7) must be solved with the following boundary conditions which apply to both fluids

$$T(0) = T_o \quad , \quad T'(0) = 0 \ , \text{ and } T(a) = T_a \quad . \tag{8}$$

These define an eigenvalue problem with the eigenvalues being the central value of the temperature for each of the two species.

The ion conductivity is assumed to be given by an anomalous thermal conductivity plus the Chang-Hinton interpolation formula [13] which is a modified version of the Hazeltine-Hinton interpolation formula [12]

$$\chi_i^{NC} = (\frac{r}{R})^{1/2} \frac{\rho_{i\theta}^2}{\tau_i} K_2 \quad , \tag{9}$$

where $\rho_{i\theta}$ is the poloidal ion Larmor radius, τ_i^{-1} is the ion-ion collision frequency, and K_2 is given by the following expression

$$K_2 = K_2^{(0)} \left[\frac{K_2^*/0.66}{1+a_2\nu_i^{*1/2}+b_2\nu_i^*} + \frac{(c_2^2/b_2)\nu_i^*(r/R)^{3/2}}{1+c_2\nu_i^*(r/R)^{3/2}} F\right] \tag{10}$$

where

$$K_2^* = \left[0.66 + 1.88 (\frac{r}{R})^{1/2} - 1.54 \frac{r}{R}\right] < \frac{B_o^2}{B^2} > ,$$

$$F = \frac{1}{2} (\frac{r}{R})^{-1/2} \left[< \frac{B_o^2}{B^2} > - < \frac{B^2}{B_o^2} >^{-1}\right] ,$$

$$< \frac{B_o^2}{B^2} > = \frac{1+3/2[(r/R)^2+(r/R)R_0']+3/8(r/R)^3R_0'}{1+(1/2)(r/R)R'_0} \quad , \tag{11}$$

$$< \frac{B^2}{B_0^2} >^{-1} = \frac{(1-r^2/R^2)^{1/2}[1+(1/2)(r/R)R_0']}{1+R_0'(r/R)^{-1}[(1-r^2/R^2)^{1/2}-1]} \quad ,$$

with $K_2^{(0)} = 0.66$, $a_2 = 1.03$, $b_2 = 0.31$, $c_2 = 0.74$, and R_0' being the Shafranov shift. In Eqs. (9) through (11) $\nu_i^* \equiv \nu_{ii}/\omega_{bi}$ is given by

$$\nu_i^* = Z_{eff} \frac{R^{3/2} B}{r^{1/2} \tau_i B_\theta (T_i/m_i)^{1/2}}$$

with

$$\tau_i = \frac{3m_i^{1/2} T_i^{3/2}}{4\pi^{1/2} ne^4 \pounds n\Lambda} \tag{12}$$

and m_i being the ion mass. The expression for the anomalous ion thermal conductivity due to the η_i mode is given by

$$\chi_i^A = \frac{5}{2} \varepsilon_n^{1/2} \eta_i^{1/2} \omega_n^* k_\perp^{-2} h(\eta_i)$$

where $k_\perp \rho_i = 0.5$ is assumed. The function $h(\eta_i)$ is approximated in our code by $h(\eta_i) = \exp(-(\eta_{crit}/\eta_i)^4)$ which is equal to one for $\eta_i > \eta_{crit}$ and to zero for $\eta_i < \eta_{crit}$. Linear theories for the η_i mode indicate a threshold for $\eta_i = \eta_{crit} \approx 1$ to 2 [24].

The electron thermal conductivity inside the q = 1 surface (as discussed in Sec. III) is given by the following semi-empirical expression

$$\chi_e = 8 \times 10^5 \, n_o^{-1}(10^{14}\mathrm{cm}^{-3}) R^{-1}(\mathrm{cm}) \, \frac{\mathrm{cm}^2}{\mathrm{sec}} \qquad r < r_1 \quad .$$

For $q > 1$, Eq. (1) is used with a correction factor which takes into account the effect of the magnetic drift destabilizing processes at low collisionality, i.e.,

$$\chi_e = \frac{5}{2} \left(\frac{r}{R}\right)^{3/2} \frac{\omega_n^* \omega_{Te}^*}{k_\perp^2} \tau_e \frac{1}{1+(0.1/\nu_e^*)} \quad . \tag{13}$$

Note that the last term in Eq. (13) is approximately unity except for very small values of ν_e^*. Finally, inside the m = 2 island, determined by the MHD model described in the next section, the electron thermal conductivity is assumed to be given by a constant sufficiently large to flatten the temperature profile inside the island. It is convenient here to introduce the following set of normalized variables

$$\rho = \frac{r}{a} \quad , \quad \hat{T}_{e(i)}(\rho) = \frac{T_{e(i)}(r)}{T_{e(i)}(0)} \quad , \quad \hat{n}(\rho) = \frac{n(r)}{n(0)}$$

$$\hat{P}_{aux}(\rho) = \frac{P_{aux}(r)}{P_{aux}(0)} \quad , \quad \hat{\chi}_{e(i)}(\rho) = \frac{\chi_{e(i)}(r)}{\chi_o}$$

where

$$\chi_o = \frac{(a/R)^{3/2} \, T_e^2(0) \tau_e(0)}{m_e^2 \, \Omega_e^2 \, a^2 \, Z_{eff}} \quad . \tag{15}$$

The quantities λ and η can be considered as the eigenvalues of Eqs. (3) to (8), i.e.,

$$\lambda = \frac{P_\Omega(0)}{n(0)T_e(0)} \frac{a^2}{\chi_o} \tag{16}$$

and

$$\eta = \frac{T_i(0)}{T_e(0)} \tag{17}$$

In such units the central electron temperature can be written as

$$T_e(0) = \bar{T}\, \lambda^{-1/6} \tag{18}$$

with

$$\bar{T} \cong 16.95\, a^{5/12}(\text{cm})\, R^{-1/12}(\text{cm}) B_T^{2/3}(\text{kG})(\ell n \Lambda)^{1/3} q_o^{-1/3} [2\gamma(Z_{eff})Z_{eff}]^{1/6} \text{ eV} ,$$

and Eqs. (3) to (8) can be expressed as

$$\lambda\, \hat{T}_e^{3/2} \hat{\sigma}_{eff} + \lambda^{3/4}\, S_{aux_e} \hat{P}_{aux_e} - \lambda^{5/6} S_\Delta \frac{\hat{n}^2}{\hat{T}_e^{3/2}} \left(\hat{T}_e - \eta\, \hat{T}_i\right) + \frac{1}{\rho} \frac{d}{d\rho} \rho\, \hat{n}\, \hat{\chi}_e \frac{d\hat{T}_e}{d\rho} = 0 \tag{19}$$

$$\lambda^{5/6} S_\Delta \frac{\hat{n}^2}{\hat{T}_e^{3/2}} \left(\hat{T}_e - \eta \hat{T}_i\right) + \lambda^{3/4}\, S_{aux_i} \hat{P}_{aux_I} + \eta \frac{1}{\rho} \frac{d}{d\rho} \rho\, \hat{n} \left[S^{NC}_{\chi_i} \lambda^{2/3}\, \eta^{-1/2}\, \hat{\chi}^{NC}_i + S^{A}_{\chi_i} \eta^{3/2} \lambda^{1/3}\, \hat{\chi}^{A}_i \right] \frac{d\hat{T}_i}{d\rho} = 0 \tag{20}$$

with

$$\hat{T}_e(0) = \hat{T}_i(0) = 1 \ , \quad \left.\frac{d\hat{T}_e}{d\rho}\right|_{\rho=0} = \left.\frac{d\hat{T}_i}{d\rho}\right|_{\rho=0} = 0, \quad \hat{T}_i(1) = \hat{T}_{ia},$$

$$\text{and } \hat{T}_e(1) = \hat{T}_{ea} \quad .$$

The parameters S_Δ, S_{aux_e}, S_{aux_i}, $S^{NC}_{\chi_i}$, and $S^{A}_{\chi_i}$ are the ratio between the ohmic heating time, $\tau_h \equiv P_\Omega(0)/n(0)T_e(0)$, and, respectively, the electron-ion equilibration time, the electron and ion auxiliary heating time and the ion (neoclassical and anomalous) confinement time. Their expressions are listed below:

$$S_\Delta = \frac{3e^2}{m_i} \frac{n_o^2 \bar{T}}{J_o^2 \gamma(Z_{eff})}$$

$$S_{aux_e} = \frac{3}{4(2\pi)^{1/2}} P_{aux_e}(0) \frac{\bar{T}^{3/2}}{J_o^2 m_e^{1/2} e^2 \ell n \Lambda \gamma(Z_{eff})} \tag{21}$$

$$S_{aux_i} = \frac{3}{4(2\pi)^{1/2}} P_{aux_i}(0) \frac{\bar{T}^{3/2}}{J_o^2 m_e^{1/2} e^2 \ell n \Lambda \gamma(Z_{eff})}$$

$$S^{NC}_{\chi_i} = \frac{16\sqrt{2}\pi}{9} (\ell n \Lambda)^2 Z_{eff} \left(\frac{m_i}{m_e}\right)^{1/2} \frac{n_o^2}{\bar{T}^4} a^2 e^8$$

$$S^{A}_{\chi_i} = \frac{5}{2} \frac{1}{k_\perp \rho_i} \frac{4(2\pi)^{1/2}}{3} \ell n \Lambda \left(\frac{m_i}{m_e}\right)^{1/2} \frac{n_o e^4 R Z_{eff}}{\bar{T}^2} \quad .$$

In addition,

$$\hat{\chi}_e(\rho) = \frac{5}{2} \rho^{3/2} \frac{\hat{n}'}{\hat{n}^2} \hat{T}_e^{5/2} \frac{d\hat{T}_e}{d\rho} \left(1 + \frac{0.1}{\nu_e^*}\right)^{-1} \quad ,$$

$$\hat{\chi}_i^{NC}(\rho) = \rho^{3/2} \frac{\hat{n}}{\hat{T}_i^{1/2}} q^2 K_2(\nu_i^* , \epsilon, \rho) \quad , \tag{22}$$

$$\hat{\chi}_i^A(\rho) = \frac{5}{2}\,\hat{\tau}_i\left(\frac{d\hat{T}_i}{d\rho}\right)^{1/2} h(n_i) \quad ,$$

and

$$\hat{\sigma}_{eff} = g\left(\frac{\rho}{\rho_1}\right) + \left[1 - g\left(\frac{\rho}{\rho_1}\right)\right]\frac{\sigma(\rho)}{\sigma(\rho_1)} \quad . \tag{23}$$

Finally, in terms of Eqs. (15) to (18) the total energy confinement time for an ohmic discharge can be written as

$$\tau_E = \frac{1.46\times10^{-20}}{(\ell n\Lambda)^{1/6}}\, n_o(cm^{-3})a^{25/24}(cm)R^{43/24}(cm)B_T^{-1/3}(kG)q_o^{7/6}$$

$$\times\, f_{OH}\left[\frac{Z_{eff}}{2\gamma(Z_{eff})}\right]^{7/12} Z_{eff}^{-1/6}\,\lambda^{-5/12} \quad , \tag{24}$$

where

$$f_{OH} = \frac{3}{2}\,\frac{\int_o^1 \rho d\rho \hat{n}(\hat{T}_e + \hat{n}\hat{T}_i)}{\int_o^1 \rho d\rho \hat{\sigma}_{eff}\hat{T}_e^{3/2}} \quad .$$

III. MHD MODEL

The effect of the m = 1 sawtooth is relevant in determining both the energy transport and the current density inside the q = 1 surface. In the present model the energy transport is described by an effective thermal conductivity χ_e^s. Using dimensional arguments it is possible to show that χ_e^s can be written as $C\, r_1^2/\tau_s$ where τ_s is the sawtooth repetition time and C is a numerical constant of order unity which takes into account the time average of the temperature profile. Using the experimentally determined [26] scaling law for τ_s [i.e., $\tau_s(msec) = (1/800)\, n_o(10^{14}cm^{-3})r_1^2(cm)R(cm)$] then gives, for C = 1,

$$\chi_e^s = \frac{8\times10^5}{n_o(10^{14}\,cm^{-3})R(cm)}\,\frac{cm^2}{sec} \qquad r < r_1 \quad . \tag{25}$$

This expression yields a value sufficiently large to cause a flattening of the temperature profile inside the q = 1 surface. The effect of the mode on the current density is to produce a fluctuating electric field in the opposite direction with respect to the field of the transformer. Such an effect limits the current density at the center so that the central safety factor does not drop to values much less than one. Due to the fact that the temperature profile is practically flattened for $q < 1$, this effect is competitive with the neoclassical correction to the Spitzer resistivity, which tends to yield $(T_e)_{r\to0} \sim T_o + \alpha r^{1/2}$ (except in a small region around the magnetic axis where $\nu^* > 1$).

Flattening the current density inside the q = 1 surface, is, of course, not equivalent to flattening the electron temperature profile if the neoclassical correction to the Spitzer resistivity is retained. Hence, in the present model, it is appropriate to define an effective conductivity given by

$$\sigma_{eff} = \begin{cases} \eta^{-1}(r) & r \geq r_1 \\ \eta^{-1}(r_1) & r \leq r_1 \end{cases} \tag{26}$$

with η given by Eq. (5).

The stability of the $m \geq 2$ tearing modes is studied solving the $\beta = 0$ equation for the helical flux function, $\psi(r)\exp[i(m\theta-kz)]$, i.e.,

$$\frac{1}{r}\frac{d}{dr}\,r\,\frac{d\psi}{dr} = \left[\frac{m^2}{r^2} + \frac{dJ_\parallel/dr}{(q_o/2)r[(1/q)-(n/m)]}\right]\psi \quad . \tag{27}$$

The mode is unstable if the quantity Δ' is greater than 0 with

$$\Delta' = \lim_{\varepsilon \to 0} \frac{\psi'(r_s+\varepsilon)-\psi'(r_s-\varepsilon)}{\psi(r_s)} \quad . \tag{28}$$

If the mode is unstable, the island width is determined by solving the following system of equations [27]

$$\Delta'(w) \equiv \frac{\psi'(r_s+x_+)-\psi'(r_s+x_-)}{\psi(r_s)} = 0 \quad ,$$

$$x_\pm = \frac{(1+s^2w^2/4)^{1/2}-1}{2s} \pm \frac{w}{2} \quad , \tag{29}$$

$$s = \frac{1}{2}\left[\psi'(r_s + x_+) + \psi'(r_s+x_-)\right] \quad ,$$

where w is the island width and s is the average derivative of ψ across the island. Due to the large parallel electron thermal conductivity we assume that the electron temperature profile is flattened inside the island. We can expect that the effect on transport of an m = 2 island is relevant only at low q_a operation. At values of q_a larger than 3 the width of the m = 2 island found without flattening the current profile is small (w/a < 0.1) and it is further reduced if the profile is flattened. At value of q_a lower than 3 a new phenomenon can occur, i.e., the interaction between the m = 1 and the m = 2 modes which has been proposed as an explanation of the hard disruptions in tokamaks [28]. However, in the present studies we are mainly interested in the steady-state behavior of the discharge rather than in the occurrence of major disruptions.

IV. METHOD OF SOLUTION AND RESULTS

Equations (19) and (20) are second order ordinary nonlinear differential

equations. However, the nonlinearity does not involve the highest order derivative, i.e., it is possible to solve explicitly for $\hat{T}''$ in terms of $\hat{T}$ and $\hat{T}'$.

To do this it is convenient to write Eq. (19) in the following form

$$\hat{p}(\lambda,\hat{T},\rho) + \frac{1}{\rho}\frac{d}{d\rho}\,\rho\,\hat{n}(\rho)\hat{\chi}(\rho,\hat{n},\hat{n}',\hat{T},\hat{T}')\,\frac{d}{d\rho}\,\hat{T} = 0 \quad .$$

Taking into account that

$$\frac{d\hat{\chi}}{d\rho} = \frac{\partial\hat{\chi}}{\partial\rho} + \frac{\partial\hat{\chi}}{\partial\hat{n}}\,\hat{n}' + \frac{\partial\hat{\chi}}{\partial\hat{n}'}\,\hat{n}'' + \frac{\partial\hat{\chi}}{\partial\hat{T}}\,\hat{T}' + \frac{\partial\hat{\chi}}{\partial\hat{T}'}\,\hat{T}''$$

then leads to

$$\left(\hat{n}\hat{\chi} + \hat{n}\hat{T}'\,\frac{\partial\hat{\chi}}{\partial\hat{T}'}\right)\hat{T}'' + \left[\hat{p}(\lambda,\hat{T},\rho) + \frac{1}{\rho}\,\hat{n}\,\hat{\chi}\hat{T}' + \hat{n}'\hat{\chi}\hat{T}'\right.$$

$$\left. + \hat{n}\,\hat{T}'\left(\frac{\partial\hat{\chi}}{\partial\rho} + \frac{\partial\hat{\chi}}{\partial\hat{n}}\,\hat{n}' + \frac{\partial\hat{\chi}}{\partial\hat{n}'}\,\hat{n}'' + \frac{\partial\hat{\chi}}{\partial\hat{T}}\,\hat{T}'\right)\right] = 0 \quad .$$

Equations (19) and (20), written in this form, are integrated from $\rho = 0$ to $\rho = 1$ with different values of λ and η until the boundary conditions are satisfied.

A. Low Density Ohmic Discharge

As already observed, the scaling law for the energy confinement time (assuming ion losses negligible) is very similar to the Neo-Alcator scaling given by Goldston [11], i.e.,

$$\tau_E = 7.1 \times 10^{-22}\,\bar{n}(\mathrm{cm}^{-3})\,a^{1.04}(\mathrm{cm})R^{2.04}(\mathrm{cm})\,q_a^{1/2}\ \mathrm{sec} \quad .$$

From Eq. (19), assuming $Z_{eff} = 1$ and observing that, if the ion losses are neglected, the eigenvalue λ can be written as $\hat{\lambda}(q_a)\ \alpha_n$, we have (for $\ell n\ \Lambda = 20$ and $q_o = 1$)

$$\tau_E = 8.5 \times 10^{-21} n_o(cm^{-3}) a^{1.04}(cm) R^{1.8}(cm) B^{-0.33}(kG) f_{OH}(q_a)(\alpha_n \hat{\lambda})^{-5/12} sec\ .$$

We note that the dependence on the magnetic field here has no practical significance since the factor $R^{0.24}B^{0.33}$ is almost constant for most machines of interest. Therefore, at low density, where the scaling with density and dimensions is satisfied, the only issue is the scaling with the edge safety factor.

On Fig. 1 (curve a) the energy confinement time is plotted against q_a. The results are in good agreement with the scaling $\tau_E \propto q_a^{\alpha}$ with $1/2 < \alpha < 1$. Another quantity, which can be studied to check the consistency of the obtained temperature profiles with the experimentally observed profiles, is the position of the $q = 1$ surface. The $q = 1$ radius has been found to be well approximated by $r_1/a = q_a^{-1}$ [29]. On Fig. 2, r_1/a is plotted as a function of q_a (curve a). In the range $2 < q_a < 4$ the agreement is fairly good, but at larger value of q_a, the agreement is worse. A direct inspection of the profiles (Fig. 3) indicates that the value of the temperature near the edge is too large. As shown in Fig. 4, this is the region where the electron thermal conductivity is underestimated. These trends can be explained as follows. At low q_a ($q_a < 3$) the bad confinement edge region (the region beyond the $q = 2$ surface) is a small fraction of the plasma column and plays a negligible role in determining the position of the $q = 1$ surface. On the other hand, at larger q_a ($q_a > 4$) this region is large. Hence, if the effects in this region

are poorly represented, the experimentally measured profiles cannot be reproduced. Nevertheless, the global confinement properties of the discharge, which are primarily governed by the physics of the good thermal insulation region between q = 1 and q = 2 surfaces, are expected to be better reproduced than the details of the profiles. This is illustrated by Fig. 1.

In order to represent properly the behavior of the electron temperature in the edge region a large electron thermal conductivity is needed. We have first investigated the possibility that such enhanced conductivity is due to the effect of the m = 2 island, using the model described in Secs. III and IV. The change in the profile is shown in Fig. 5 for the same parameters and safety factor of Fig. 3. These results indicate that the effect of the m = 2 mode provides only a small change in the temperature profile and does not lead to the proper behavior of the temperature in the edge region. It is most important to emphasize here that the effect of the m = 2 island is really significant only at low values of q_a. At large values of q_a it is necessary to invoke another mechanism for enhanced transport in the q > 2 region. This is illustrated in Fig. 6 which shows the location of the q = 2 surface, the m = 2 island extension, and the position of the q = 1 surface for various edge safety factors.

In order to reproduce the experimental trends at high q_a we need to introduce an appropriate transport model for the region q > 2. As explained in Sec. I such a model is provided by Eq. (2). The improved results for τ_E and r_1/a vs. q_a are shown on Figs. 1 and 2 as curve b. In Fig. 7 the corresponding temperature profiles for electrons and ions and the thermal conductivities are shown for a high q_a case.

At low q_a values, the current density profile between the q = 1 and the q = 2 surfaces has a steep gradient which leads to a large increase in the

width of the satured island and, eventually, to a major disruption [28]. Such behavior depends strongly on the value of q on axis and, therefore, on the details of the model for the m = 1 sawtooth. In Fig. 8 the temperature and current density profiles for a case with a large m = 2 island are shown.

B. High Density Ohmic Discharges

After finding reasonable agreement between the model and the experimental results at low density, where the electron losses dominate, we next focused our attention on the ion losses. Four different machines have been considered. First we have applied our model to the Alcator A machine (the 150 kA discharges considered in Ref. 30). This device is characterized by an increasing peakedness of the density profile with increasing density (α_n = 0.75 + 0.25[1. - $\bar{n}(10^{14}cm^{-3})$]). As a result, the toroidal η_i mode does not play a role in affecting the global energy transport. The experimental results from Ref. 14 for τ_E vs. $\bar{n}$ are shown on Fig. 9. It might be argued that the good agreement here could be due in part to neglecting loss terms, such as radiation, which can be important (even if not dominant) in these discharges. Nevertheless, the results confirm that the general trend of the experimental results are well reproduced by our model.

The second device we have considered is the Doublet III [5] machine whose results, as already noted, cannot be explained by the usual ion neoclassical theory. In particular, the cases studied here involve the 473 kA discharges with a = 44 cm, and are characterized by a flattening of the density profile as the average density increases (Fig. 5 of Ref. 5). This behavior is quite different from that observed in Alcator A where the density becomes more peaked as the average density increases. Since flatter density profiles imply larger values of η_i, we accordingly expect that with increasing $\bar{n}$ a continuous

increase in the level of turbulence of the η_i mode should be generated. The results for the Doublet III discharges are shown in Fig. 10 where the electron energy replacement time, $\tau_{Ee} \equiv \int dV(3/2)nT_e/\int dVP_\Omega$, is plotted against $\bar{n}$ (curve a). The black circles represent the experimental data from Fig. 6 of Ref. 5. Here it is demonstrated that the effect of the η_i mode is to establish a plateau at high densities in agreement with the observed trend. As illustrated in Fig. 10 this agreement cannot be produced if the η_i mode is turned off. Similar conclusions have been obtained in independent studies using a time-dependent transport code [31]. The behavior of the ion temperature profile, when the η_i mode is destabilized, can be understood by observing that, due to the fact that the anomalous χ_i is much larger than the neoclassical value, the profile adjusts itself to be near the marginally stable situation. As a result, the quantity η_i/η_{crit}, appears to be constant across the main part of the discharge, except in a narrow region around the center and close to the edge. A good analytic approximation to the ion temperature profile is $T_i = T_i(0)(1-r^2/a^2)^{\alpha_{Ti}}$ where $\alpha_{Ti} = \eta_{crit}\ \alpha_n$. Such conclusion is quite general and is applicable to other machines where the η_i instabilities are present.

Similar results have been found for the Alcator C device. In Fig. 11 we have compared the discharges with a = 10 cm, R = 64 cm, B_T = 12 T, and I = 270 kA [Fig. 1(c) of Ref. 7] assuming Z_{eff} = 1.2 and α_n = 0.5 for all these cases. The results are again in agreement with the experimental values which fall well below the low density scaling trend for τ_E.

Finally, we have considered the results of the ohmic discharges of the PDX experiment [32]. Figure 13 shows reasonable agreement between the results of the code and the experimental results [Fig. 9(f) of Ref. 32].

In concluding this section we want to stress that no adjustable

parameters have been used in the results presented. Therefore, the fact that the agreement found for very different situations is more than qualitative provides strong support for the model proposed here for the ion losses.

V. CONCLUSIONS

In this paper we have presented a model for anomalous energy transport in ohmically heated tokamaks. With regard to the specific types of mechanisms invoked, the transport in the $q < 1$ region is mainly due to the sawtooth activity, the electron transport in the region between the $q = 1$ and the $q = 2$ surfaces is due to the dissipative trapped electron mode turbulence, and a semi-empirical model has been assumed in the region beyond the $q = 2$ surface. The ion thermal conductivity is given by the Chang and Hinton formula plus an anomalous χ_i due to the effect of the toroidal η_i mode.

The main conclusions of our work can be summarized as follows:

(1) At low density the presented transport model gives results in reasonable agreement with the Neo-Alcator scaling for τ_E and with the results of the profile-consistent microinstability model of Ref. 23. While low q_a discharges are insensitive to the choice of the local transport effects in the edge region, additional physics in this zone is required to describe properly the high q_a discharges. Such additional information, however, does not seem to be related to the effect of the $m = 2$ mode which is relevant only at low q_a.

(2) At high densities the effect of the toroidal η_i mode provides an explanation for the early saturation of the energy confinement time observed under very different experimental situations.

ACKNOWLEDGMENT

Valuable discussions with Dr. J. W. Connor concerning the formulation of the basic model are gratefully acknowledged.

This work supported by United States Department of Energy Contract No. DE-AC02-76-CHO-3073.

REFERENCES

[1] GAUDREAU, M., GONDHALEKAR, A., HUGHES, M. H., OVERSKEI, D., PAPPAS, D. S., et al., Phys. Rev. Lett. 39 (1977) 1266.

[2] JASSBY, D. L., COHN, D. R.., PARKER, R. R., Nucl. Fusion 16 (1976) 1045.

[3] PFEIFFER W., WALTZ, R. E., Nucl. Fusion 19 (1979) 51.

[4] MURAKAMI, M., NEILSON, G. H., HOWE, H. C., JERNIGAN, T. C., BATES, S. C., et al., Phys. Rev. Lett. 42 (1979) 655.

[5] EJIMA, S., PETRIE, T. W., RIVIÈRE, A. C., ANGEL, T. R., ARMENTROUT, C. J., et al., Nucl. Fusion 22 (1982) 1627.

[6] FAIRFAX, S., GONDHALEKAR, A., GRANETZ, R., GREENWALD, M., GWINN, D., et al.,in Plasma Physics and Controlled Nuclear Fusion Research 1980 (Proc. 8th Int. Conf. Brussels, 1980),Vol. 1, IAEA, Vienna, (1981) 439.

[7] BLACKWELL, B., FIORE, C. L., GANDY, R., GONDHALEKAR, A., GRANETZ, R. S., et al., in Plasma Physics and Controlled Nuclear Fusion Research 1982 (Proc. 9th Int. Conf. Baltimore, 1982), Vol. 2, IAEA, Vienna (1983) 27.

[8] EQUIPE TFR, Nucl. Fusion 20 (1980) 1227.

[9] ALLADIO, F., BARDOTTI, G., BARTIROMO, R., BUCETI, G., BURATTI, P. et al., Nucl.. Fusion 22 (1982) 479.

[10] HUGILL, J., Nucl. Fusion 23 (1983) 331.

[11] GOLDSTON, R. J., Plasma Phys. 26 (1984) 87.

[12] HINTON, F. L., HAZELTINE, R. D., Rev. Mod. Phys. 48 (1976) 239.

[13] CHANG, C. S., HINTON, F. L., Phys. Fluids 25 (1982) 1493.

[14] GONDHALEKAR, A., OVERSKEI, D., PARKER, R., WEST, S., WOLFE, S., Energy Confinement in Alcator, MIT Report No. PFC/RR-79-6 (June 1979).

[15] KADOMTSEV, B. B., POGUTSE, O. P., Nucl. Fusion 11 (1971) 67.

[16] TANG, W. M., Nucl. Fusion 18 (1978) 1089.

[17] CONNOR, J. M., HASTIE, R. J., TAYLOR, J. B., Proc. R. Soc. (London), Ser. A1 (1979) 365.

[18] CHEN, LIU, CHENG, C. Z., Phys. Fluids 23 (1980) 2242.

[19] REWOLDT, G., TANG, W. M., FRIEMAN, E. A., Phys.. Fluids 21 (1978) 1513.

[20] LIEWER, P., Nucl. Fusion 25 (1985) 543.

[21] COPPI, B., Comments Plasma Phys. Controlled Nucl. Fusion 5 (1980) 261.

[22] PERKINS, F. W., in Heating in Toroidal Plasmas (Proc. of the 4th Joint Varenna - Grenoble Int. Symp. Rome, 1984) Vol. 2, Int. School of Plasma Physics, Perugia (1984) 977.

[23] TANG, W. M., Microinstability-Based Model for Anomalous Thermal Confinement in Tokamaks Princeton University Plasma Physics Laboratory Report PPPL-2311 (1986).

[24] GUZDAR, P. N., CHEN, LIU, TANG, W. M., RUTHERFORD, P. H., Phys. Fluids 26 (1983) 673.

[25] GREENWALD, M., GWINN, D., MILORA, S., PARKER, J., PARKER, R. et al., Phys. Rev. Lett. 53 (1984) 352.

[26] Equipe TFR, Plasma Physics and Controlled Nuclear Fusion Research 1976 (Proc. 6th Int. Conf. Berchtesgaden, 1976) Vol. 1, IAEA, Vienna, (1977) 279.

[27] WHITE, R. B., MONTICELLO, D. A., ROSENBLUTH, M. N., WADDELL, B. V., Phys. Fluids 20 (1977) 800.

[28] TURNER, M. F., WESSON, J. A., Nucl. Fusion 22 (1982) 1069.

[29] DIVA Group Nucl. Fusion 20 (1980) 271.

[30] LIEWER, P. C., PFEIFFER, W., WALTZ, R. E., Phys. Fluids 26 (1983) 563.

[31] DOMINGUEZ, R. R., WALTZ, R. E., Tokamak Transport Code Simulations with Drift Wave Model GA Technologies Inc. Report GA-A18184 (1986).

[32] BOL, K., ARUNASALAM, V., BITTER, M., BOYD, D., BRAU, K., et al., in Plasma Physics and Controlled Nuclear Fusion Research 1978 (Proc. 7th Int. Conf. Innsbruck, 1978), Vol. 1, IAEA, Vienna (1979), 11.

FIGURE CAPTIONS

FIG. 1. Energy confinement time τ_E (in arbitrary units) vs edge safety factor q_a for $n(0) = 2 \times 10^{13} cm^{-3}$. Parameters are those of the Doublet III machine with B = 24 kG, R = 143 cm, a = 44 cm, $Z_{eff} = 1$, and $\alpha_n = 1$. Curves (a) and (b) refer, respectively, to the case without and with the edge model. The Neo-Alcator curve, $\tau_E \propto q_a^{1/2}$, is also shown for comparison.

FIG. 2. Position of q = 1 surface, r_1/a, vs edge safety factor q_a for the same parameters as Fig. 1. Curves (a) and (b) refer, respectively, to the case without and with the edge model. The curve $r_1/a = q_a^{-1}$ is also shown for comparison.

FIG. 3. Temperature profiles vs r/a for electrons (curve a) and ions (curve b) for the same parameters as Fig. 1 and for various q_a. The curve c) represents a Gaussian temperature profile corresponding to the same value of q_a.

FIG. 4. Thermal conductivities vs r/a for the same parameters as Fig. 3 and for various q_a. The curves are labelled as follows: (a) electron thermal conductivity, (b) ion thermal conductivity, (c) INTOR thermal conductivity, (d) Goldston thermal conductivity, (e) Tang thermal conductivity.

FIG. 5. Temperature profiles vs r/a for electrons (curve a) and ions (curve b) for the same parameters as Fig. 1 and various q_a with the effect of the m = 2 island included. The curve c) represents a Gaussian temperature profile corresponding to the same values of q_a.

FIG. 6. Positions of the q = 1, q = 2 surface and island width vs q_a for the same parameters as Fig. 1. The curves a) and b) correspond, respectively, to the case with and without the edge model.

FIG. 7. Temperature profile vs r/a for electrons (curve a) and ions (curve b) for the same parameters as Fig. 1 and various q_a with the edge model included. The curve c) represents a Gaussian temperature profile corresponding to the same value of q_a.

FIG. 8. Temperature and current density profiles for the same parameters as Fig. 1 and a large value of the m = 2 island.

FIG. 9. Global energy confinement time vs $\bar{n}$ for the Alcator A parameters a = 10 cm, R = 54 cm, B_T = 60 kG, Z_{eff} = 1.4, and I = 150 kA. The variation of the exponent α_n characterizing the density profile is also displayed. The black circles are the experimental results and the open circles are the results of the transport code.

FIG. 10. Electron energy confinement time vs $\bar{n}$ for the Doublet III parameters a = 44 cm, R = 143 cm, B_T=24 kG, and I = 473 kA. The black circles are the experimental results and the open circles (curve a) are the results of the transport code. Curve b) represents the results with the η_i mode turned off. The variation of the exponent α_n characterizing the density profile and of the parameter Z_{eff} is also shown.

FIG. 11. Global energy confinement time vs $\bar{n}$ for the Alcator C parameters a = 10 cm, R = 64 cm, B_T = 120 kG, I = 270 kA, Z_{eff} = 1.2, and α_n = 0.5.

FIG. 12. Electron energy confinement time vs $\bar{n}$ for the PDX parameters a = 40 cm, R = 130 cm, B_T = 32 kG, I = 450 kA, Z_{eff} = 1, and α_n = 1.

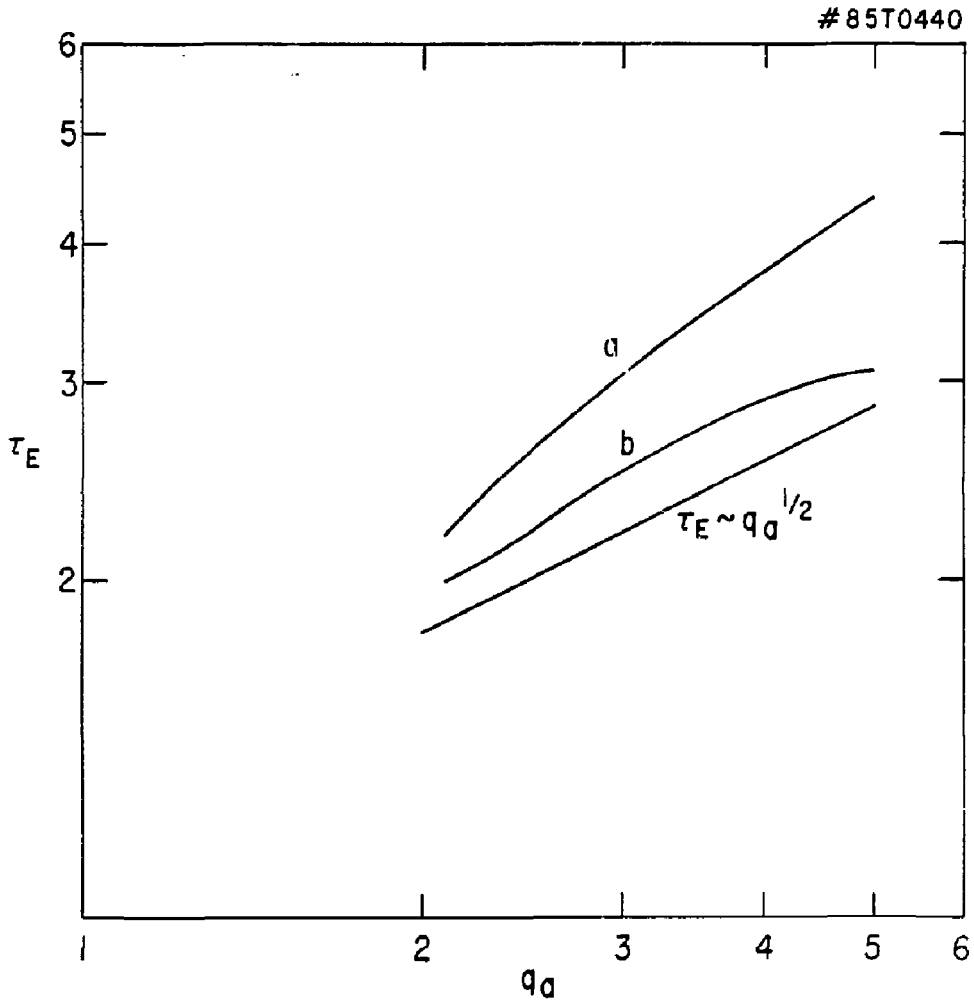

Fig. 1

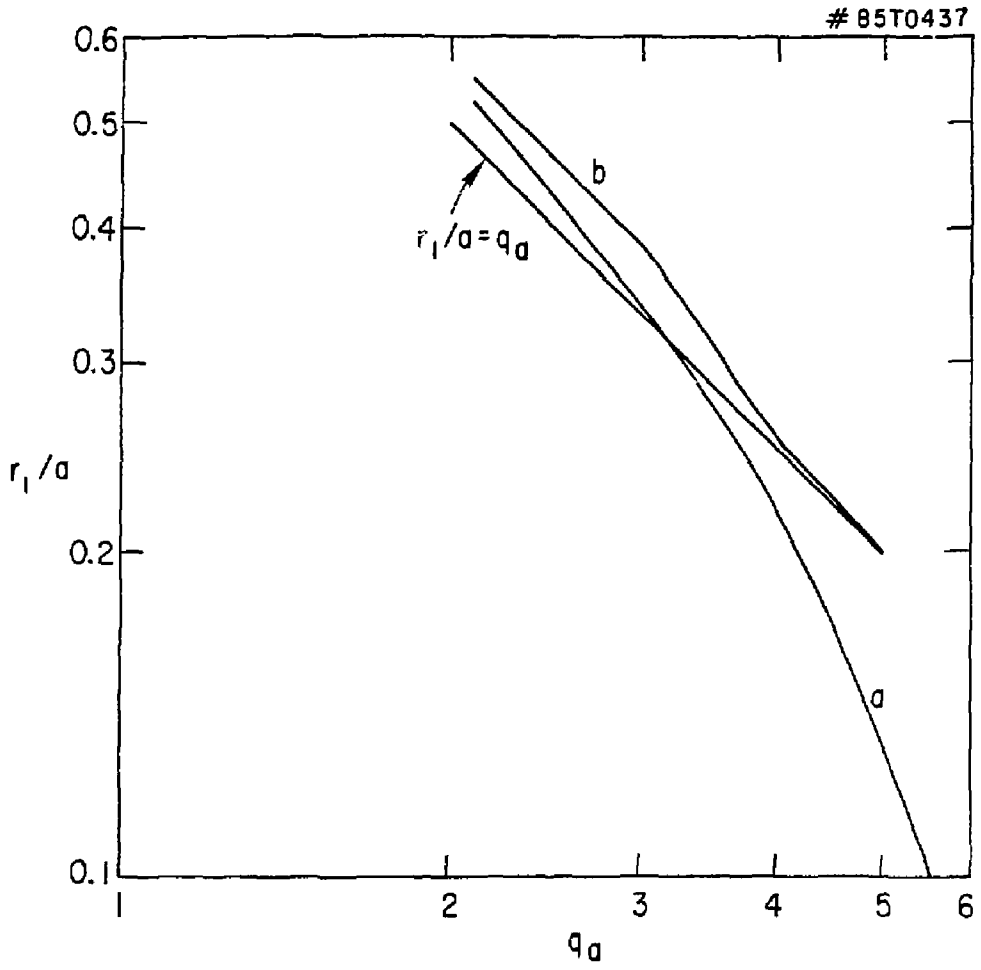

Fig. 2

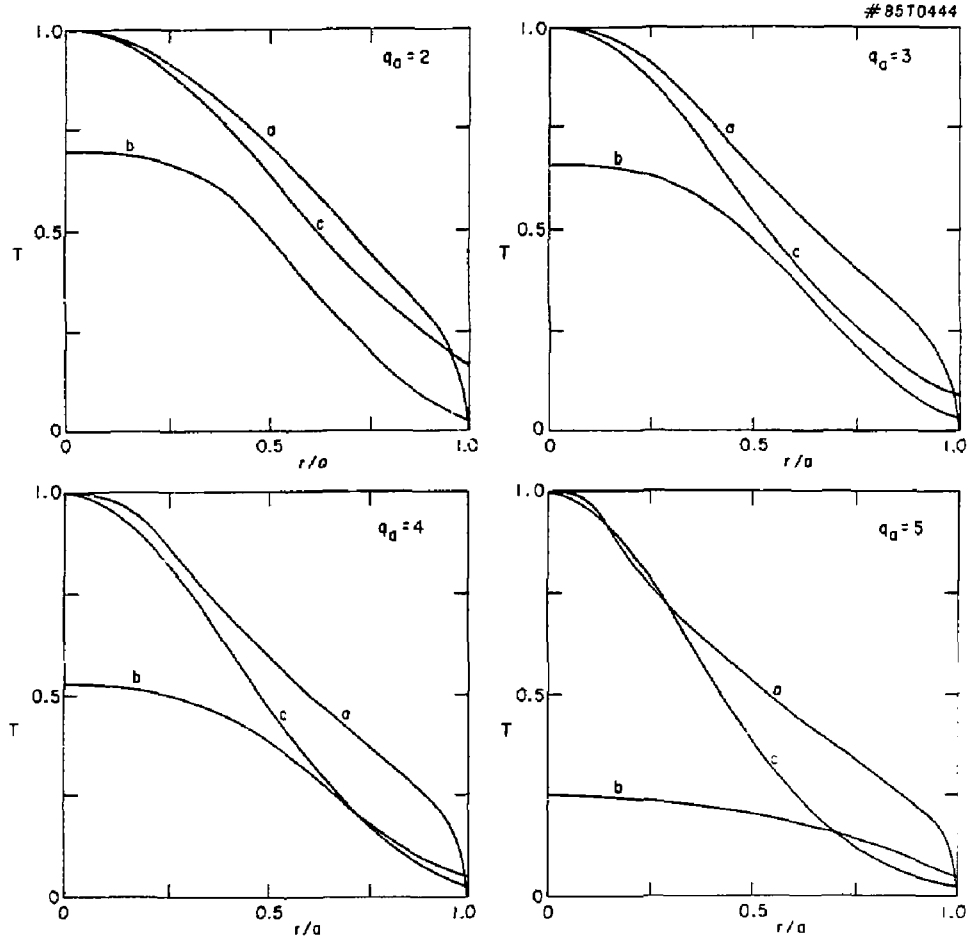

Fig. 3

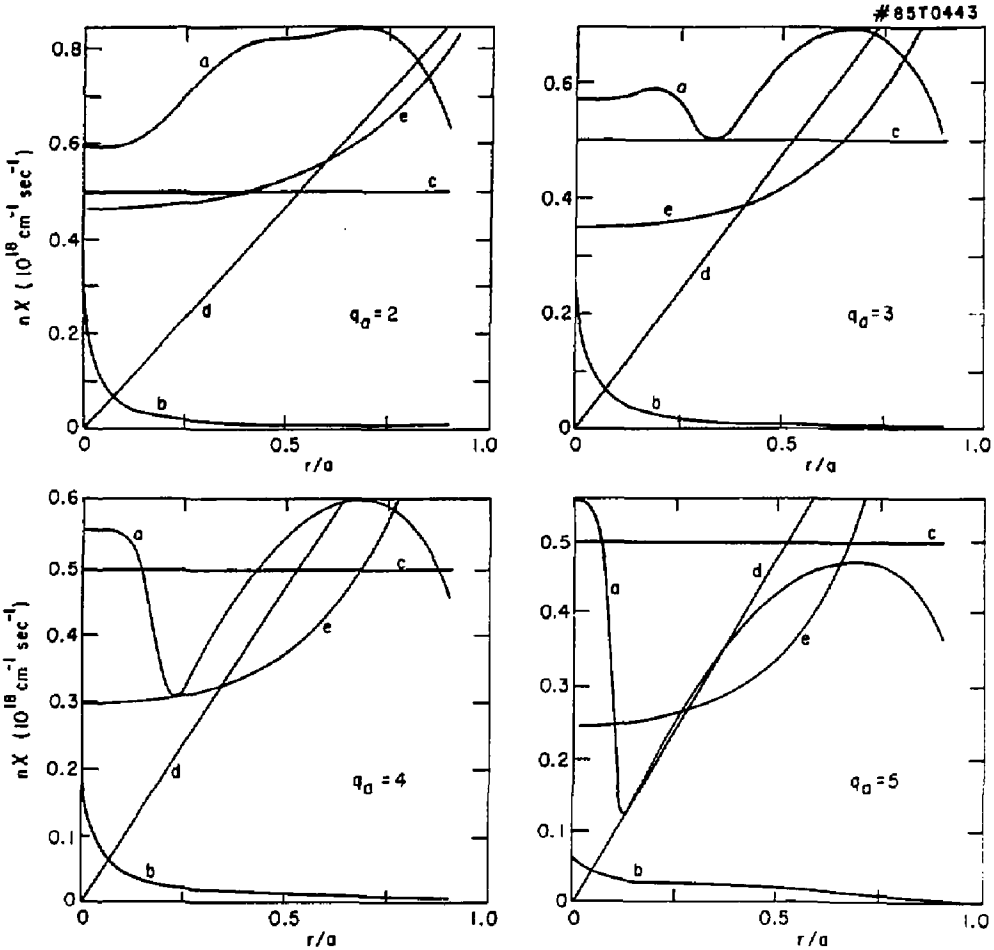

Fig. 4

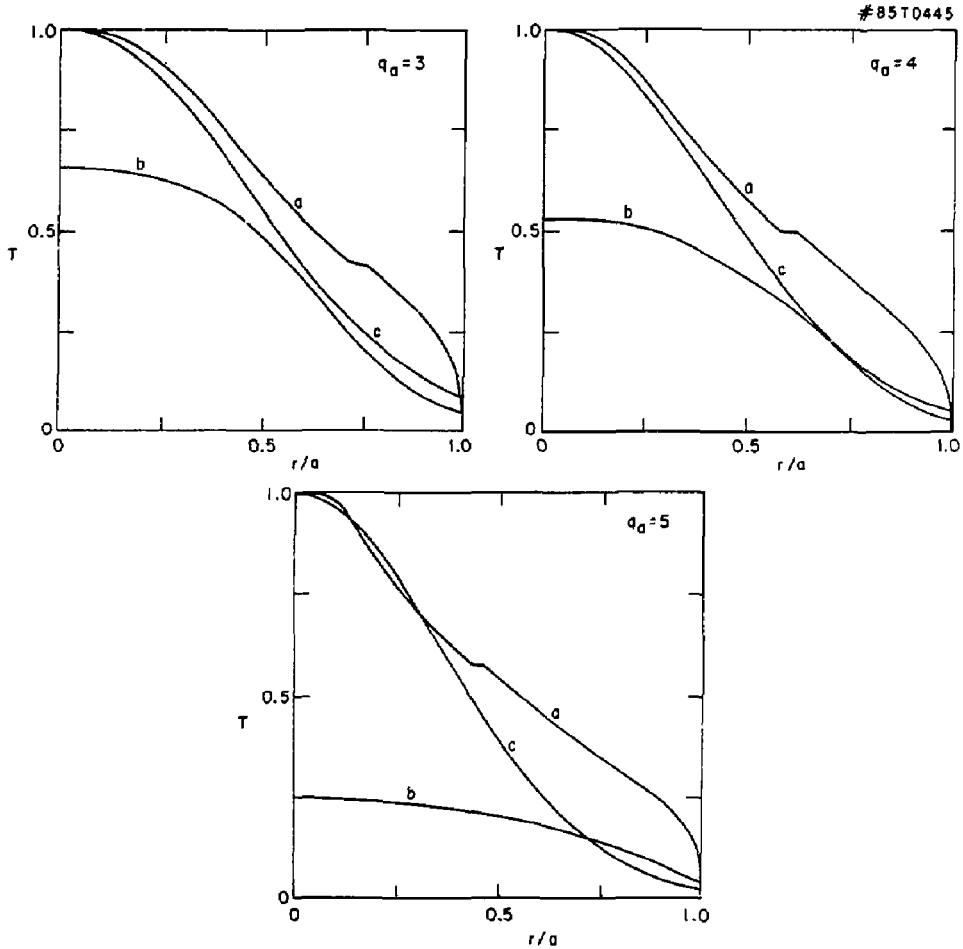

Fig. 5

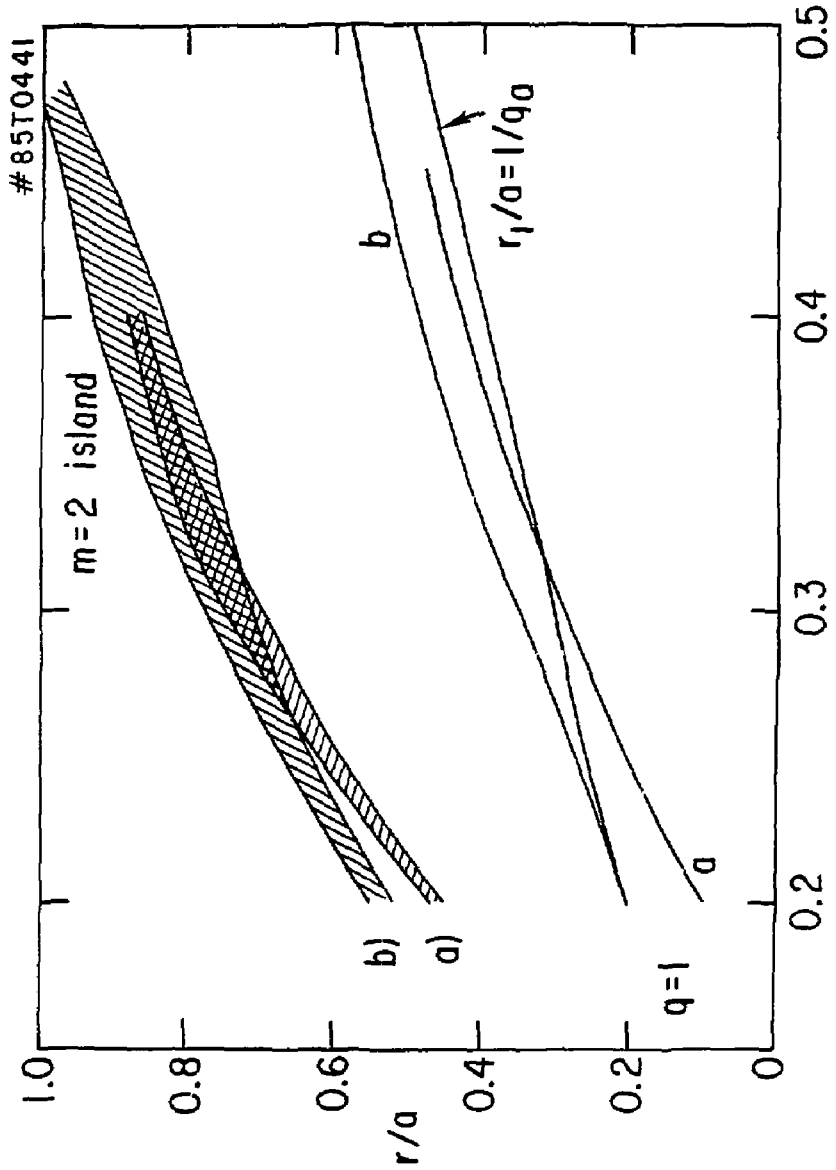
#85T0441
m=2 island
b
a
$r_1/a=1/q_a$
q=1
a
b)
a)
r/a
1.0
0.8
0.6
0.4
0.2
0
0.2
0.3
0.4
0.5
$1/q_a$

Fig. 6

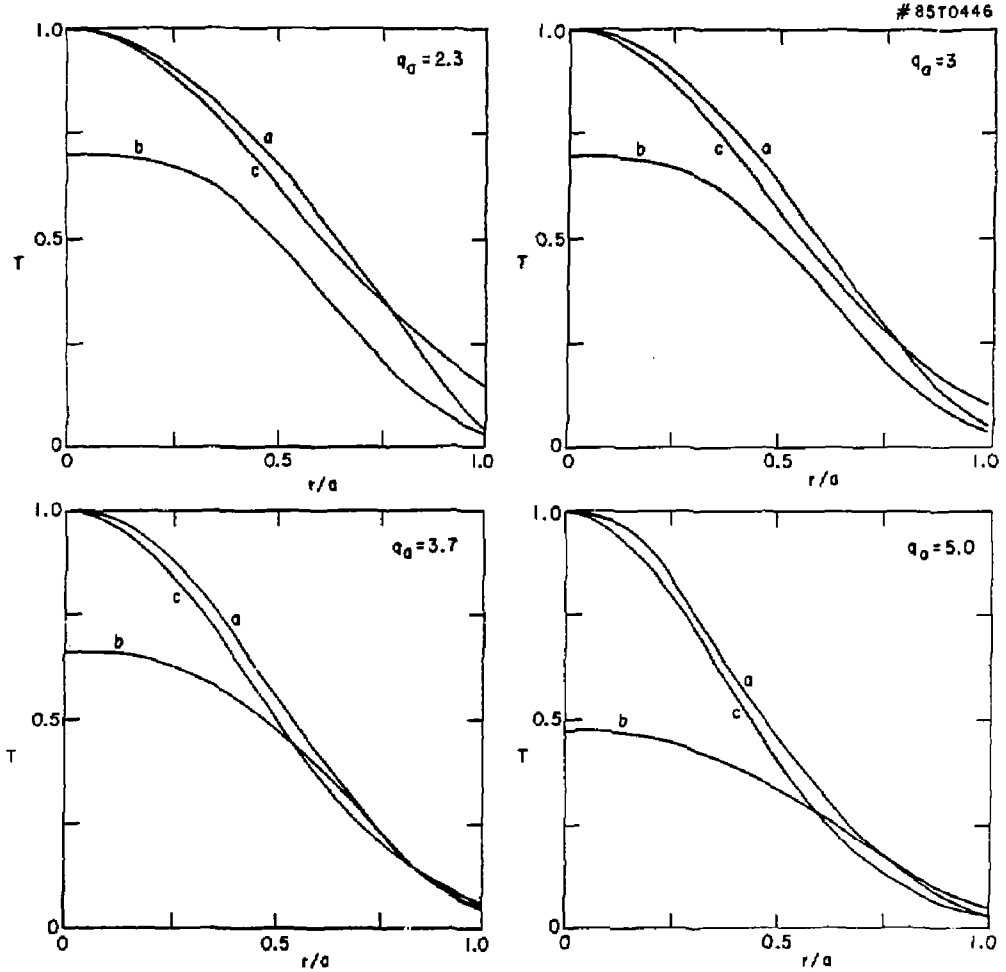

Fig. 7

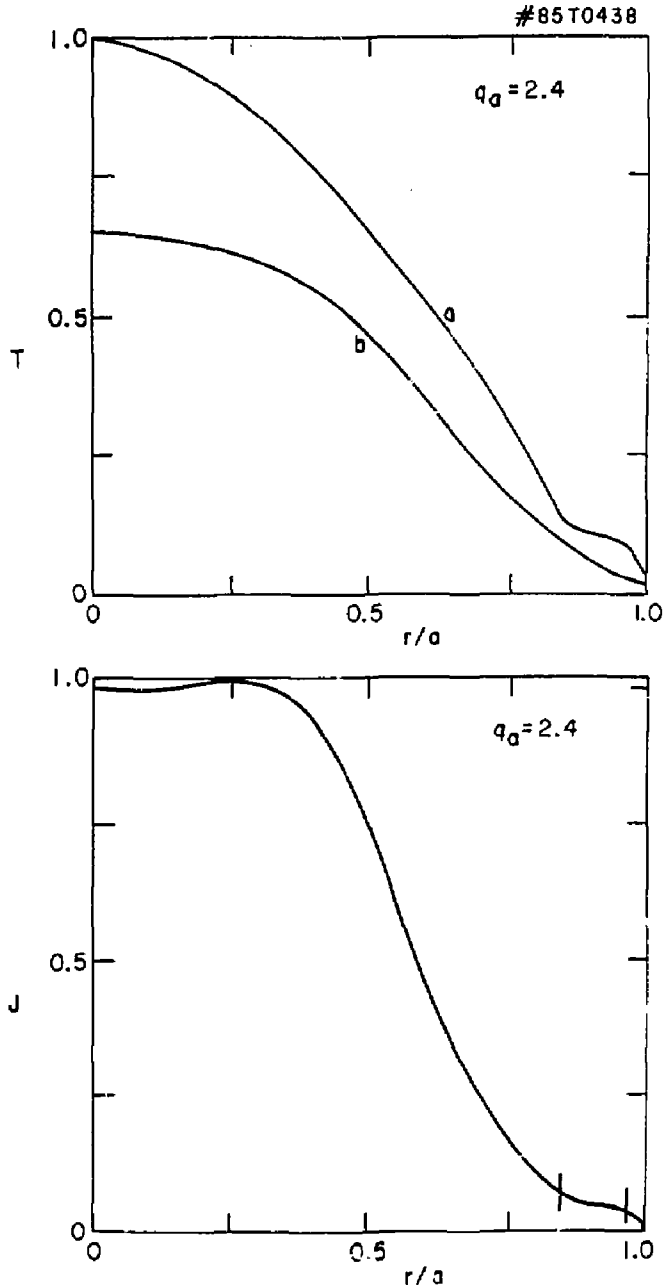

Fig. 8

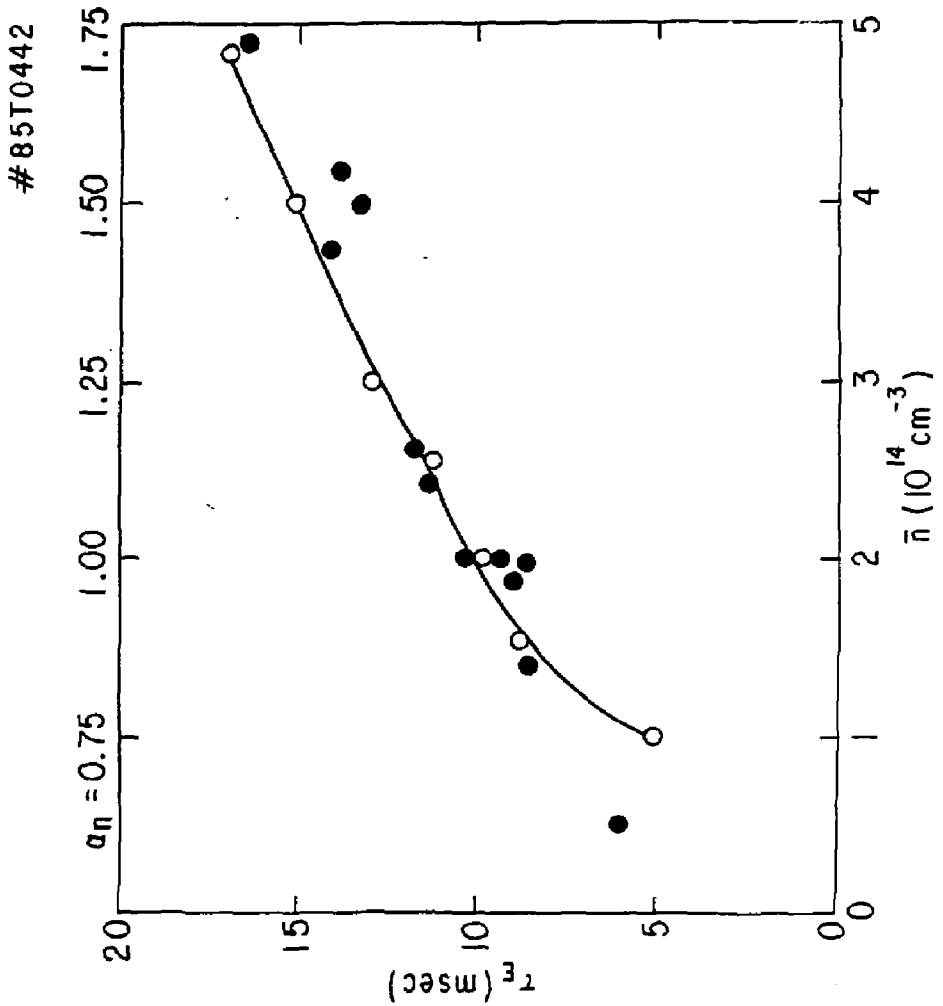
#85T0442
$a_n = 0.75$
τ_E (msec)
$\bar{n}$ (10^{14} cm^{-3})
0
5
10
15
20
1.00
1.25
1.50
1.75
1
2
3
4
5

Fig. 9

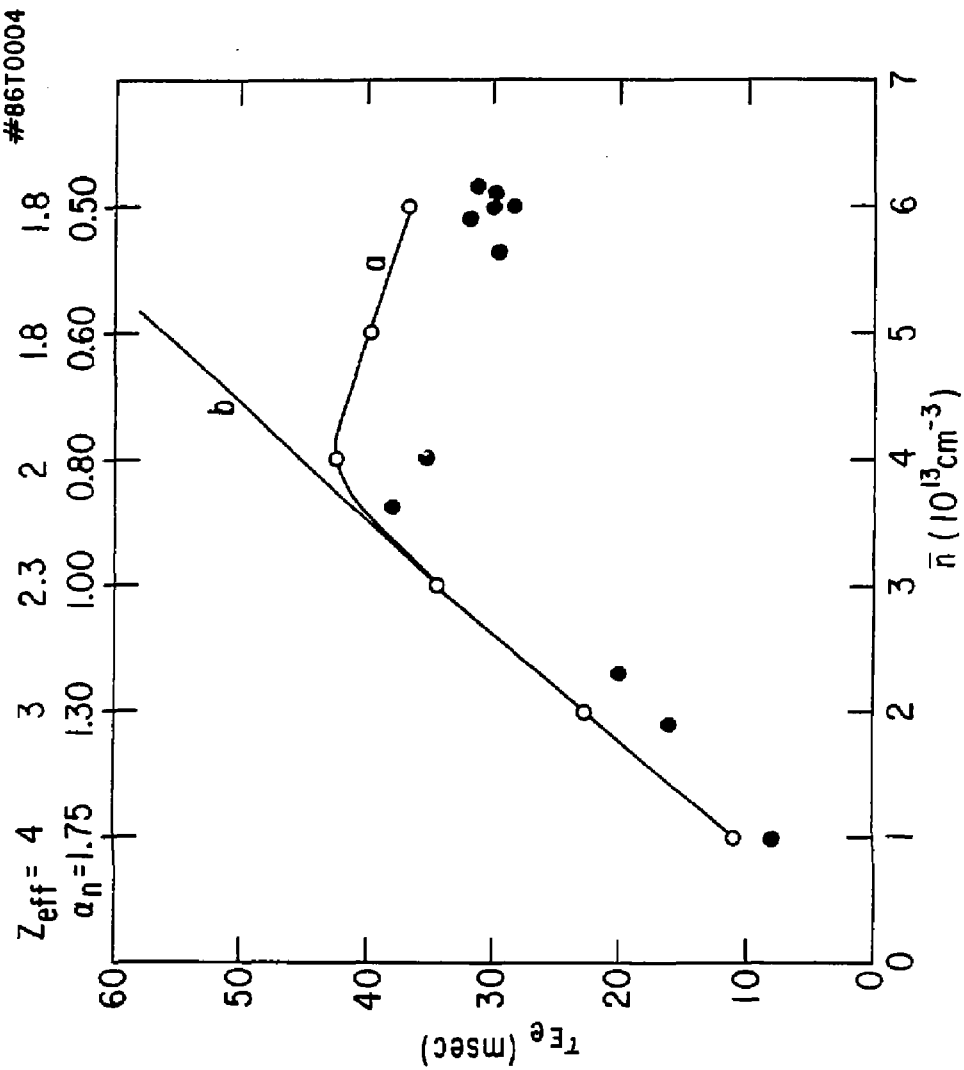
#86T0004
Z_{eff}= 4 3 2.3 2 1.8 1.8
a_n=1.75 1.30 1.00 0.80 0.60 0.50
a
b
τ_{Ee} (msec)
$\bar{n}$ (10^{13}cm^{-3})
0 10 20 30 40 50 60
0 1 2 3 4 5 6 7

Fig. 10

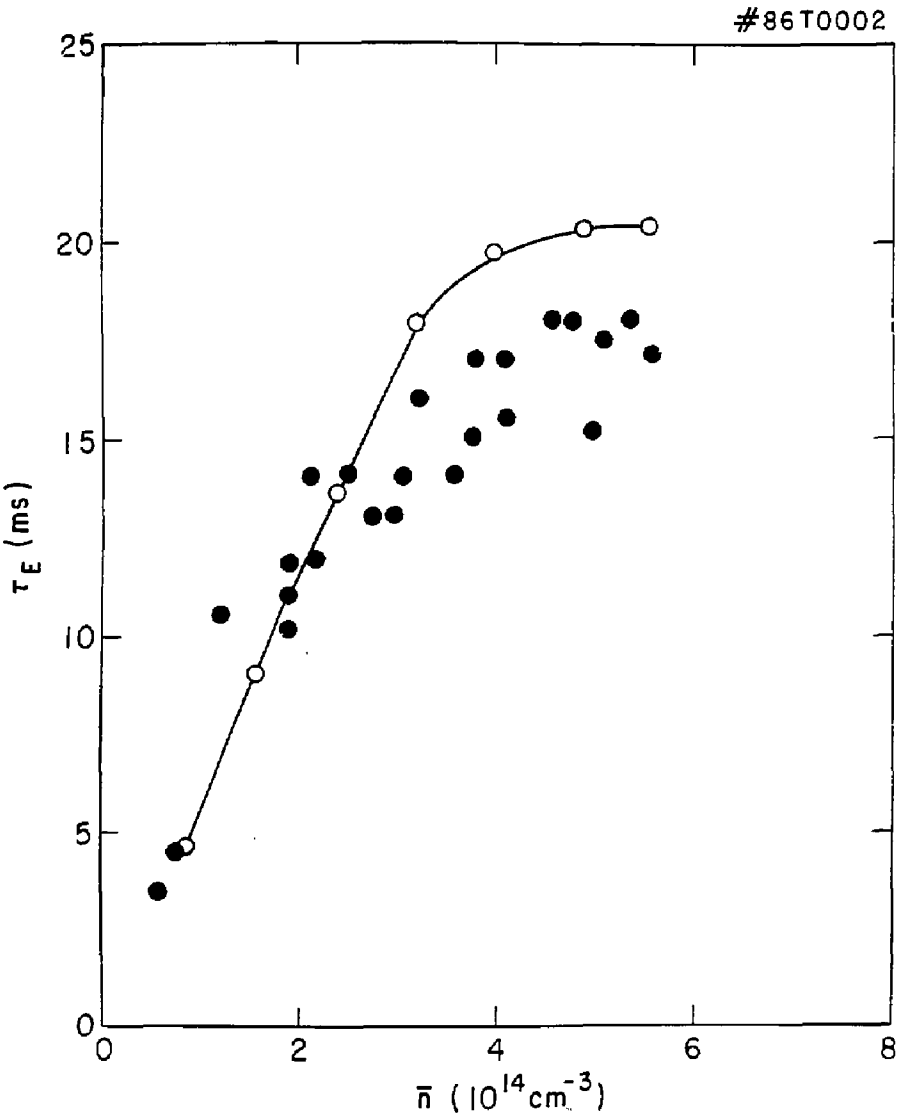

Fig. 11

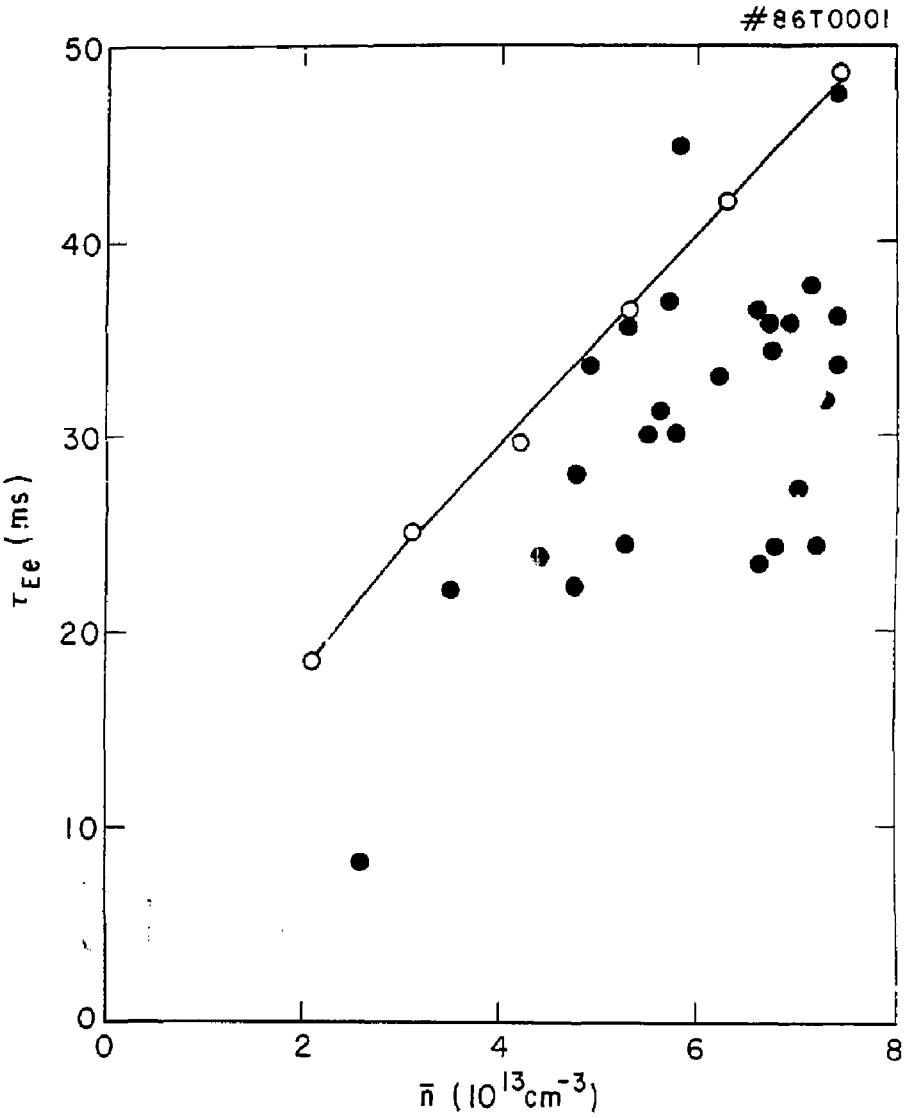

Fig. 12